

The following article has been submitted to *The Journal of Chemical Physics*.

©2021 Hiroki Kusudo. This article is distributed under a Creative Commons Attribution (CC BY) License.

Local stress tensor calculation by the Method-of-Plane in microscopic systems with macroscopic flow: a formulation based on the velocity distribution function

Hiroki Kusudo,^{1, a)} Takeshi Omori,^{2, b)} and Yasutaka Yamaguchi^{1, 3, c)}

¹⁾*Department of Mechanical Engineering, Osaka University, 2-1 Yamadaoka, Suita 565-0871, Japan*

²⁾*Department of Mechanical and Physical Engineering, Osaka City University, 3-3-138 Sugimoto, Sumiyoshi-ku, Osaka 558-8585, Japan*

³⁾*Water Frontier Research Center (WaTUS), Research Institute for Science & Technology, Tokyo University of Science, 1-3 Kagurazaka, Shinjuku-ku, Tokyo, 162-8601, Japan*

(Dated: 19 July 2021)

In this work, we showed a calculation method of local stress tensor applicable to non-equilibrium MD systems based on the Method of Plane (MoP). From the relation between the macroscopic velocity distribution function and the microscopic molecular passage across a fixed control plane, we derived a method to calculate the basic properties of the macroscopic momentum conservation law including the density, the velocity, the momentum flux, the interaction and kinetic terms of the stress tensor defined on a surface with a finite area. Any component of the streaming velocity can be obtained on a control surface, which enables the separation of the kinetic momentum flux into the advection and stress terms in the framework of MoP. We verified the present method through the extraction of the density, velocity and stress distributions in a quasi-1D steady-state Couette flow system and in a quasi-2D steady-state system with a moving contact line. In our method, as opposed to volume average method, the density, mass and momentum fluxes are defined on a surface, which is essential to be consistent with the mass and momentum conservation laws in dynamic systems.

^{a)}Electronic mail: hiroki@nfm.mech.eng.osaka-u.ac.jp

^{b)}Electronic mail: omori@osaka-cu.ac.jp

^{c)}Electronic mail: yamaguchi@mech.eng.osaka-u.ac.jp

I. INTRODUCTION

With the increasing interest in microfluidic devices and nanotechnologies, molecular dynamics (MD) simulations have become a powerful computational tool to examine the fluid behavior for small scale systems. For the understanding in terms of flow fields, the microscopic motion of individual molecules must be averaged, and the stress tensor plays a key role in such macroscopic flow. Within the framework of fluid mechanics, the stress tensor is determined from the velocity fields through the constitutive equation typically including the viscosity, and the local acceleration of the fluid is given by the gradient of the stress tensor as well as the external field to satisfy the momentum conservation. On the other hand, the molecular motion is governed by the intermolecular interaction, and the stress tensor should be defined through the average of the molecular motion and interaction.

More concretely, the macroscopic equation of continuity is given with the density $\rho(\mathbf{x}, t)$ and velocity vector $\mathbf{u}(\mathbf{x}, t)$ both as functions of position \mathbf{x} and time t by

$$\frac{\partial \rho}{\partial t} + \frac{\partial \rho u_k}{\partial x_k} = 0, \quad (1)$$

where x_k and u_k are the k -direction components of the position and the velocity vector, respectively. The Einstein notation is used with a dummy index k for the vectors. The second term of the LHS is called the advection or streaming term. Equation (1) comes from the mass conservation

$$\iiint_V dV \frac{\partial \rho}{\partial t} = - \iint_S dS \rho u_k n_k \quad (2)$$

satisfied for an arbitrary volume V in an enclosing surface S , where n_k is the k -direction component of the outward unit normal vector \mathbf{n} with respect to the infinitesimal surface element dS . This integral form in Eq. (2) means that the mass in V can be changed only by the mass flux passing the surface S . By applying Gauss' divergence theorem for the RHS as

$$\iint_S dS \rho u_k n_k = \iiint_V dV \frac{\partial \rho u_k}{\partial x_k}, \quad (3)$$

it follows for Eq. (2) that

$$\iiint_V dV \left(\frac{\partial \rho}{\partial t} + \frac{\partial \rho u_k}{\partial x_k} \right) = 0, \quad (4)$$

for an arbitrary V , which corresponds to Eq. (1).

Similarly, the macroscopic momentum equation, the Navier-Stokes equation, is given by

$$\frac{\partial \rho u_l}{\partial t} + \frac{\partial \rho u_l u_k}{\partial x_k} = \frac{\partial \tau_{kl}}{\partial x_k} + \rho F_l, \quad (5)$$

where the fluid stress tensor component τ_{kl} expresses the stress in the l -direction exerted on a surface element with an outward normal in the k -direction, and F_l denotes the external force per mass. This is also derived from the momentum conservation for an arbitrary volume V enclosed by S :

$$\iiint_V dV \frac{\partial \rho u_l}{\partial t} = - \iint_S dS \rho u_l u_k n_k + \iint_S dS \tau_{kl} n_k + \iiint_V dV \rho F_l, \quad (6)$$

meaning that the total momentum in V can be changed by the momentum flux passing the surface S as well as the impulse due to the stress exerted on the surface S and external force exerted on the volume V . Specifically note that the advection $\rho u_l u_k$ and stress τ_{kl} in the 1st and 2nd terms of the RHS, respectively, are separated.

In contrast to the above-mentioned macroscopic feature, microscopic molecules have their own velocities, and their local average and variance correspond to the macroscopic velocity \mathbf{u} and temperature under the assumption of local equilibrium in space and time, respectively. Hence, an instantaneous microscopic mass or momentum transfer across an arbitrary surface S exists due to the passage of the constituent molecules even in macroscopically static system without mean flow with $\mathbf{u} = \mathbf{0}$. In the kinetic theory of gases based on the Boltzmann equation with respect to the velocity distribution function (VDF) of the constituent molecules, the macroscopic velocity is subtracted from the microscopic molecular velocity upon the definition of the stress. Before the establishment of the MD method, Irving and Kirkwood¹ (IK) put forward the connection between the macroscopic conservation laws and microscopic molecular motion governed by the inter-molecular interaction through the statistical mechanical theory based on the distribution function in the phase space, and derived an expression of the local pointwise stress comprised of kinetic and interaction parts including Taylor series expansion of differences in delta functions to express the microscopic particle feature.

After the introduction of numerical MD simulations,^{2,3} the calculation of average stress in homogeneous bulk systems, equivalent to the average bulk pressure with its sign inverted, was enabled based on the virial theorem, which indeed corresponds to the average of the IK form integrated in space and time. From this bulk stress, the viscosity as a transport

coefficient can also be obtained based on the Green-Kubo relation from the time-fluctuation of the off-diagonal stress component averaged in space.^{4,5} Regarding the local stress implemented for MD simulations with a discrete time-step, Tsai⁶ proposed a pragmatic scheme to calculate the averaged stress defined on a flat plane in quasi-1D planer systems, and Thompson *et al.*⁷ extended the approach toward a spherical curved surface for the analysis of the surface tension of a spherical droplet. In both cases, all the momentum flux and intermolecular force across the plane or the sphere, which divide the computational domain, were summed up during the time integration in macroscopically static systems. This type of stress definition is usually called the Method of Plane (MoP),⁸ or Hardy⁹ stress, where the momentum conservation law with the above-mentioned MoP for quasi-1D systems was proved to be an exact consequences of Newton’s laws,⁹ *i.e.*, the MoP meets Gauss’ divergence theorem for any control volume (CV) surrounded by enclosing surface(s) irrespective of whether the local system in the control volume is homogeneous or not. In addition, this momentum conservation is not restricted to quasi-1D systems but also applicable to quasi-2D systems, *e.g.*, the present authors adopted the MoP for a CV with an rectangular enclosing surface set around the contact line of an equilibrium droplet to examine the nanoscale wetting behavior through the mechanical balance exerted on the fluid in the CV.¹⁰ On the other hand, the volume average (VA) is proposed as another approach that gives the local mean stress in space, where weighted average of the pair interaction in local CVs is included in the formulation.^{11–19} This VA should in principle be applied only for homogeneous CVs, and is advantageous especially to explore the link with the local fluctuation and thermodynamic limit,^{16,17} while stress integral can also be obtained by the VA, and this enables the calculation of the surface tension based on Bakker’s equation using this stress integral,²⁰ which is known as a mechanical route to evaluate the surface tension.^{5,12,19,21–23} The momentum conservation is satisfied for the whole system if the VA is properly summed up; however, special care is needed to consider the momentum conservation for local CVs because the VA originally was not designed to examine local momentum conservation to be satisfied through the link to Gauss’ divergence theorem.^{9,14,18} This feature is similar to the atomic stress,²⁴ for instance provided as *stress/atom* command in LAMMPS package,²⁵ often used to simply visualize the stress field.

Going back to the momentum conservation in Eq. (6), for systems with a non-zero local flow, *i.e.*, macroscopically dynamic systems with $\mathbf{u} \neq \mathbf{0}$, the local macroscopic velocity \mathbf{u}

must be defined on a surface S enclosing a control volume V in MD systems so that the stress calculated in MD simulations may be consistent with the macroscopic momentum Eq. (5). In other words, the momentum transfer due to the microscopic molecular passage across a control surface should be separated into advection and stress contributions to examine the local flow from a macroscopic point of view.

In this paper, we show a calculation method of the MoP-based local stress tensor applicable to non-equilibrium molecular dynamics (NEMD) systems. We provide the formulation for systems consisting of single-component mono-atomic fluid molecules for simplicity while the present framework is also applicable to systems of multi-component or poly-atomic fluid molecules. For the derivation, we introduced the VDF to clearly give the average of physical properties defined on a fixed control plane as we shall see later. With this procedure, we provide not only the expression of the kinetic term of stress tensor but also those of the components in the advection term, *i.e.*, the density and macroscopic velocity as an extension of the MoP. To check its validity, we performed test calculation in two systems: 1) a quasi-1D Couette flow system and 2) a quasi-2D system with liquid-solid-vapor contact lines, both consisted of a Lennard-Jones fluid between parallel solid walls moving in the opposite directions tangential to the walls. In the first system, we compared the density and velocity distributions obtained by the present method and the VA, and we calculated the distributions of the stress components and advection term. Furthermore, we showed that the same velocity distribution was obtained on bin faces with different normal directions, which is essential to determine the advection term. In the second system, the density, velocity and stress distributions are calculated in the complex flow with liquid-vapor interfaces and contact lines.

II. THEORY

We show the derivation of the stress averaged on a finite bin face in a Cartesian coordinate system for single-component mono-atomic fluid in the following for simplicity. Note that the Einstein notation with dummy indices used in Sec. I is not applied hereafter. The fluid stress tensor component τ_{kl} which expresses the stress in the l -direction exerted on a surface element with an outward normal in the k -direction, is given by the kinetic term τ_{kl}^{kin} and the

inter-molecular interaction term τ_{kl}^{int} as

$$\tau_{kl} = \tau_{kl}^{\text{kin}} + \tau_{kl}^{\text{int}}. \quad (7)$$

In the standard MoP for equilibrium MD systems without mean flow consisting of single-component mono-atomic fluid molecules,^{8,10} the kinetic term τ_{kl}^{kin} in Eq. (7) on a bin face of area S_k with its normal vector pointing to the k -th Cartesian direction is calculated by

$$\tau_{kl}^{\text{kin}} \equiv -\frac{1}{S_k \delta t} \left\langle \sum_{i \in \text{fluid}, \delta t}^{\text{across } S_k} m^i v_l^i \frac{v_k^i}{|v_k^i|} \right\rangle, \quad (8)$$

where m^i and v_l^i denote the mass and l -component of the velocity vector \mathbf{v}^i of fluid particle i , respectively. We also denote the bin face by S_k hereafter. The angular brackets denote the ensemble average, and the summation $\sum_{i \in \text{fluid}, \delta t}^{\text{across } S_k}$ is taken for every fluid particle i passing through S_k within a time interval of δt , which is equal to the time increment for the numerical integration. Considering that we deal with a single-component fluid molecules of an identical mass m , we substitute m^i with m hereafter. A sign function $\frac{v_k^i}{|v_k^i|}$ equal to ± 1 is multiplied to the momentum transfer $m v_l^i$ across S_k to evaluate the kinetic effect on the stress depending on the passing direction. Note that in static equilibrium systems, *i.e.*, systems without macroscopic local mean flow, the advection term is zero in the whole system.

On the other hand, the intermolecular interaction term τ_{kl}^{int} in Eq. (7) in the case of simple two body potential is calculated by

$$\tau_{kl}^{\text{int}} = -\frac{1}{S_k} \left\langle \sum_{(i,j) \in \text{fluid}}^{\text{across } S_k} F_l^{ij} \frac{r_k^{ij}}{|r_k^{ij}|} \right\rangle, \quad (9)$$

where r_k^{ij} and F_l^{ij} denote the k -component of the relative position vector $\mathbf{r}^{ij} \equiv \mathbf{x}^j - \mathbf{x}^i$ and the l -component of the force vector \mathbf{F}^{ij} on particle j at position \mathbf{x}^j from particle i at position \mathbf{x}^i , respectively. The summation $\sum_{(i,j) \in \text{fluid}}^{\text{across } S_k}$ is taken for all line segments of the inter-particle interaction between \mathbf{x}^i and \mathbf{x}^j which cross S_k . A sign function $\frac{r_k^{ij}}{|r_k^{ij}|}$ is multiplied for this interaction term to evaluate the force effect depending on the force direction. Note that technically the fluid-solid interaction can also be included as i - j pair in the summation $\sum_{(i,j)}^{\text{across } S_k}$ in Eq. (9), but only the fluid-fluid interaction was taken into account as the fluid stress, and fluid-solid contribution was considered as an external force field.^{10,26,27} Also note that for multi-component systems or systems with poly-atomic molecules, difficulties mainly arise to treat the interaction force between different kind of molecules or the constraint force²⁸

of the polyatomic molecules, where the interaction forces should be properly implemented into the stress calculation to satisfy the conservation laws.²⁹

To extend the standard MoP to steady-state NEMD systems with a non-zero macroscopic mean local flow, the mean velocity should be properly subtracted from the kinetic term τ_{kl}^{kin} in Eq. (8) so that the macroscopic momentum flux as the advection term due to the mean velocity \mathbf{u} may be included not in the stress term but in the advection term within the macroscopic description of the momentum conservation, *i.e.*, in the Navier-Stokes equation (5). In the following, we provide a general framework to connect a microscopic variable ξ^i of particles and a macroscopic field value $\xi(\mathbf{x}, t)$ averaged on S_k under non-zero mean velocity based on the local VDF in the Cartesian xyz -coordinate system.

At first, we define the VDF $f(\mathbf{x}, \mathbf{v}, t)$ for the mass with a velocity $\mathbf{v} = (v_x, v_y, v_z)$ at position $\mathbf{x} = (x, y, z)$ at time t , which gives the local density $\rho(\mathbf{x}, t)$ by

$$\rho(\mathbf{x}, t) = \int_{-\infty}^{\infty} dv_x \int_{-\infty}^{\infty} dv_y \int_{-\infty}^{\infty} dv_z f(\mathbf{x}, \mathbf{v}, t) \equiv \iiint_{-\infty}^{\infty} d\mathbf{v} f(\mathbf{x}, \mathbf{v}, t), \quad (10)$$

where we rewrite $\int_{-\infty}^{\infty} dv_x \int_{-\infty}^{\infty} dv_y \int_{-\infty}^{\infty} dv_z$ by $\iiint_{-\infty}^{\infty} d\mathbf{v}$. Then a microscopic variable ξ^i per mass of particle i can be related to a corresponding macroscopic field variable $\xi(\mathbf{x}, t)$ as

$$\lim_{\delta t \rightarrow 0} \left\langle \sum_{i \in \text{fluid}, \delta t}^{\text{crossing } S_k} m \xi^i \right\rangle \equiv \lim_{\delta t \rightarrow 0} \iiint_{-\infty}^{\infty} d\mathbf{v} \int_0^{|v_k| \delta t} dx_k S_k f(\mathbf{x}, \mathbf{v}, t) \xi(\mathbf{x}, t). \quad (11)$$

The RHS denotes the integral weighted with VDF considering an oblique pillar of a base area S_k and a height $|v_k| \delta t$ with its central axis parallel to \mathbf{v} , which is typically assumed upon the derivation of the equilibrium pressure in the kinetic theory of gases.

With the limit $\delta t \rightarrow 0$, and by rewriting the average of $f(\mathbf{x}, \mathbf{v}, t)$ and $\xi(\mathbf{x}, t)$ in the oblique pillar by $f(S_k, \mathbf{v}, t)$ and $\xi(S_k, t)$, respectively, the integral with respect to x_k in the RHS of Eq. (11) writes

$$\lim_{\delta t \rightarrow 0} \int_0^{|v_k| \delta t} dx_k S_k f(\mathbf{x}, \mathbf{v}, t) \xi(\mathbf{x}, t) = \lim_{\delta t \rightarrow 0} S_k f(S_k, \mathbf{v}) \xi(S_k) |v_k| \delta t, \quad (12)$$

and it follows for Eq. (11) that

$$\lim_{\delta t \rightarrow 0} \left\langle \sum_{i \in \text{fluid}, \delta t}^{\text{crossing } S_k} m \xi^i \right\rangle = \lim_{\delta t \rightarrow 0} S_k \iiint_{-\infty}^{\infty} d\mathbf{v} f(S_k, \mathbf{v}, t) \xi(S_k, t) |v_k| \delta t. \quad (13)$$

Hence, by dividing both sides by $S_k \delta t$,

$$\iiint_{-\infty}^{\infty} d\mathbf{v} f(S_k, \mathbf{v}, t) \xi(S_k, t) |v_k| = \lim_{\delta t \rightarrow 0} \frac{1}{S_k \delta t} \left\langle \sum_{i \in \text{fluid}, \delta t}^{\text{crossing } S_k} m \xi^i \right\rangle \quad (14)$$

is derived as a basic equation for the connection between the macroscopic field variable $\xi(S_k, t)$ and microscopic variable ξ^i which belongs to the constituent particle i upon crossing S_k .

Now, we proceed to the expressions of the macroscopic field variables averaged on S_k . By substituting $\xi(S_k, t)$ and ξ^i in Eq. (14) with $\frac{1}{|v_k|}$ and $\frac{1}{|v_k^i|}$, respectively, and using Eq. (10), it follows

$$\rho(S_k, t) = \lim_{\delta t \rightarrow 0} \frac{1}{S_k \delta t} \left\langle \sum_{i \in \text{fluid}, \delta t}^{\text{crossing } S_k} \frac{m}{|v_k^i|} \right\rangle, \quad (15)$$

where v_k^i denotes the velocity component in the k -direction of particle i . Similarly, regarding the macroscopic mass flux ρu_l given by

$$\rho u_l(\mathbf{x}, t) = \iiint_{-\infty}^{\infty} d\mathbf{v} f(\mathbf{x}, \mathbf{v}, t) v_l, \quad (16)$$

substituting $\xi(S_k, t)$ and ξ^i in Eq. (14) with $\frac{v_l}{|v_k|}$ and $\frac{v_l^i}{|v_k^i|}$, respectively, leads to

$$\rho u_l(S_k, t) = \lim_{\delta t \rightarrow 0} \frac{1}{S_k \delta t} \left\langle \sum_{i \in \text{fluid}, \delta t}^{\text{crossing } S_k} \frac{m v_l^i}{|v_k^i|} \right\rangle. \quad (17)$$

From Eqs. (15) and (17), the macroscopic velocity u_l results in

$$u_l(S_k, t) = \frac{\rho u_l(S_k, t)}{\rho(S_k, t)} = \lim_{\delta t \rightarrow 0} \frac{\left\langle \sum_{i \in \text{fluid}, \delta t}^{\text{crossing } S_k} \frac{m v_l^i}{|v_k^i|} \right\rangle}{\left\langle \sum_{i \in \text{fluid}, \delta t}^{\text{crossing } S_k} \frac{m}{|v_k^i|} \right\rangle}. \quad (18)$$

Finally, to write the kinetic contribution of the stress τ_{kl}^{kin} , we use the expression in the kinetic theory of gases given by

$$\tau_{kl}^{\text{kin}}(\mathbf{x}, t) = - \iiint_{-\infty}^{\infty} d\mathbf{v} f(\mathbf{x}, \mathbf{v}, t) (v_k - u_k(\mathbf{x}, t)) (v_l - u_l(\mathbf{x}, t)). \quad (19)$$

By expanding Eq. (19), it follows

$$\begin{aligned} \tau_{kl}^{\text{kin}}(\mathbf{x}, t) &= - \iiint_{-\infty}^{\infty} d\mathbf{v} f(\mathbf{x}, \mathbf{v}, t) v_k (v_l - u_l(\mathbf{x}, t)) + u_k(\mathbf{x}, t) \iiint_{-\infty}^{\infty} d\mathbf{v} f(\mathbf{x}, \mathbf{v}, t) (v_l - u_l(\mathbf{x}, t)) \\ &= - \iiint_{-\infty}^{\infty} d\mathbf{v} f(\mathbf{x}, \mathbf{v}, t) v_k (v_l - u_l(\mathbf{x}, t)) + u_k \rho u_l(\mathbf{x}, t) - u_k \rho u_l(\mathbf{x}, t) \\ &= - \iiint_{-\infty}^{\infty} d\mathbf{v} f(\mathbf{x}, \mathbf{v}, t) v_k (v_l - u_l(\mathbf{x}, t)). \end{aligned} \quad (20)$$

Hence, by substituting $\xi(S_k, t)$ and ξ^i in Eq. (14) with $-\frac{v_k(v_l - u_l)}{|v_k|}$ and $-\frac{v_k^i(v_l^i - u_l)}{|v_k^i|}$, respectively, it follows

$$\begin{aligned}
\tau_{kl}^{\text{kin}}(S_k, t) &= \lim_{\delta t \rightarrow 0} \left[-\frac{1}{S_k \delta t} \left\langle \sum_{i \in \text{fluid}, \delta t}^{\text{crossing } S_k} \frac{m v_k^i (v_l^i - u_l(S_k, t))}{|v_k^i|} \right\rangle \right] \\
&= \lim_{\delta t \rightarrow 0} \left(-\frac{1}{S_k \delta t} \left\langle \sum_{i \in \text{fluid}, \delta t}^{\text{crossing } S_k} \frac{m v_k^i v_l^i}{|v_k^i|} \right\rangle + u_l(S_k, t) \frac{1}{S_k \delta t} \left\langle \sum_{i \in \text{fluid}, \delta t}^{\text{crossing } S_k} \frac{m v_k^i}{|v_k^i|} \right\rangle \right) \\
&= -\lim_{\delta t \rightarrow 0} \frac{1}{S_k \delta t} \left\langle \sum_{i \in \text{fluid}, \delta t}^{\text{crossing } S_k} \frac{m v_k^i v_l^i}{|v_k^i|} \right\rangle + \rho u_l u_k(S_k, t), \tag{21}
\end{aligned}$$

where Eq. (17) is used in the final equality. Note that the second term in the rightmost-HS can be obtained by

$$\rho u_l u_k(S_k, t) = \frac{\rho u_l(S_k, t) \cdot \rho u_k(S_k, t)}{\rho(S_k, t)} \tag{22}$$

using Eqs. (17) and (18), which correspond to the advection term in the macroscopic momentum conservation in the Navier-Stokes equation (5). By subtracting $\rho u_l u_k(S_k, t)$ from the rightmost-HS and leftmost-HS of Eq. (21), it follows

$$\tau_{kl}^{\text{kin}}(S_k, t) - \rho u_l u_k(S_k, t) = -\lim_{\delta t \rightarrow 0} \frac{1}{S_k \delta t} \left\langle \sum_{i \in \text{fluid}, \delta t}^{\text{crossing } S_k} \frac{m v_k^i v_l^i}{|v_k^i|} \right\rangle, \tag{23}$$

meaning that the microscopic total momentum transfer in the RHS corresponds to the stress minus the advection term in the LHS. Technically, the summation in the RHS of Eq. (23) is calculated during the MD simulation, and as the post process, the stress $\tau_{kl}^{\text{kin}}(S_k, t)$ is obtained by adding the advection term $\rho u_l u_k$ to the total microscopic momentum transfer as

$$\tau_{kl}^{\text{kin}}(S_k, t) = [\tau_{kl}^{\text{kin}}(S_k, t) - \rho u_l u_k(S_k, t)] + \rho u_l u_k(S_k, t), \tag{24}$$

where the advection term is calculated by the dividing $\rho u_l(S_k, t) \cdot \rho u_k(S_k, t)$ by the density $\rho(S_k, t)$ as in Eq. (22): all obtained also as the post process.

The relation between the macroscopic variables in Eqs. (1) and (5) corresponding microscopic expressions are summarized in TABLE I.

In practice, within the framework of MD, δt ($\rightarrow 0$) must be replaced by a small non-zero time step of Δt for the numerical integration. Upon this procedure without this limit, we have to assume the following: 1) the change of the distribution function $f(\mathbf{x}, \mathbf{v}, t)$ within

TABLE I. Microscopic expressions for the calculation of the corresponding macroscopic properties defined as the average on bin face S_k in steady-state systems. The top four properties can be directly calculated from steady-state systems through the MoP procedure, whereas the others below are derived from the four.

macroscopic property	microscopic expression	corresponding equation(s)
$\rho(S_k, t)$	$\lim_{\delta t \rightarrow 0} \frac{1}{S_k \delta t} \left\langle \sum_{i \in \text{fluid}, \delta t}^{\text{crossing } S_k} \frac{m}{ v_k^i } \right\rangle$	Eq. (15)
$\rho u_l(S_k, t)$	$\lim_{\delta t \rightarrow 0} \frac{1}{S_k \delta t} \left\langle \sum_{i \in \text{fluid}, \delta t}^{\text{crossing } S_k} \frac{m v_l^i}{ v_k^i } \right\rangle$	Eq. (17)
$\tau_{kl}^{\text{int}}(S_k, t)$	$-\frac{1}{S_k} \left\langle \sum_{(i,j) \in \text{fluid}}^{\text{across } S_k} F_l^{ij} \frac{r_k^{ij}}{ r_k^{ij} } \right\rangle$	Eq. (9)
$\tau_{kl}^{\text{kin}}(S_k, t) - \rho u_l u_k(S_k, t)$	$-\lim_{\delta t \rightarrow 0} \frac{1}{S_k \delta t} \left\langle \sum_{i \in \text{fluid}, \delta t}^{\text{crossing } S_k} \frac{m v_k^i v_l^i}{ v_k^i } \right\rangle$	Eq. (23)
$u_l = \frac{\rho u_l}{\rho}$	-	Eq. (18)
$\rho u_l u_k$	-	Eq. (22)
$\tau_{kl}^{\text{kin}} = (\tau_{kl}^{\text{kin}} - \rho u_l u_k) + \rho u_l u_k$	-	Eq. (24)
$\tau_{kl} = \tau_{kl}^{\text{kin}} + \tau_{kl}^{\text{int}}$	-	Eq. (7)

the distance range of $|\mathbf{v}|\delta t$ is negligibly small, and 2) the values of v_k^i and v_l^i upon ‘crossing’ should be properly evaluated based on the position update procedure of particles depending on the time integration scheme. For the velocity Verlet method, which is applied in the numerical test in Sec. III, we adopted $\mathbf{v}^i \equiv \frac{\mathbf{x}^i(t+\Delta t) - \mathbf{x}^i(t)}{\Delta t}$ using the positions $\mathbf{x}^i(t)$ and $\mathbf{x}^i(t + \Delta t)$ of fluid particle i at time t and $t + \Delta t$ before and after crossing the bin face to avoid the discrepancy of the mass flux by the MoP calculation and by the position update.

Note that Eq. (23) without the limit $\delta t \rightarrow 0$ is the same as the RHS of Eq. (8), which simply sums up the momentum transfer across the bin face S_k with a sign function $\frac{v_k^i}{|v_k^i|}$. Hence, if one locates a control volume with a closed surface consisting of the MoP bin faces, then the momentum conservation is strictly satisfied with Eq. (23). Different choices are indeed possible to determine the advection term $\rho u_l u_k(S_k, t)$ in Eq. (22) to separate the stress $\tau_{kl}^{\text{kin}}(S_k, t)$ from $\tau_{kl}^{\text{kin}}(S_k, t) - \rho u_l u_k(S_k, t)$ by Eq. (24), and this may sound that the definition of $\tau_{kl}^{\text{kin}}(S_k, t)$ is not unique. However; by setting $l = k$ in Eq. (17), the surface normal mass flux is evaluated as the simple sum of the mass passage with a sign function

$\frac{v_k^i}{|v_k^i|}$, and this strictly satisfies the mass conservation in Eq. (2), meaning that one can choose a unique definition of $\rho u_l u_k(S_k, t)$ that simultaneously satisfies the macroscopic mass and momentum conservation.

Another point to be noted is that the final forms in Eqs. (15), (17) and (23) are formally equivalent to the MoP expressions by Daivis, Travis, and Todd³⁰, which were derived for a quasi-1-dimensional flow through the expressions of the time derivative of the fluxes in a control volume with the Fourier transform, and were in principle applicable for the average on an infinite plane under a periodic boundary condition. On the other hand, our non-flux-based derivation with a definition of physical properties averaged on a face through the VDF enables the calculation of physical properties on a finite area. In addition, taking advantage of this non-flux-based feature, one can calculate, for instance, the velocity component u_l on a bin face S_k ($l \neq k$) tangential to the velocity component by Eq. (18). This point will be discussed more in detail with a quasi-1D Couette-type flow in Sec. III A as an example.

III. NUMERICAL TEST

The extended MoP was tested through the calculation of the density, macroscopic mean velocity and stress distributions in two systems with a Lennard-Jones (LJ) fluid: a quasi-1D Couette-type flow and a quasi-2D shear flow with solid-liquid-vapor contact lines. Note that both systems are in steady state and we applied time average instead of ensemble average.

A. Quasi-1D Couette-type flow

Figure 1 (a) shows the MD simulation system of a quasi-1D Couette-type flow, where the basic setup is a standard one similar to our previous study.^{31,32} The two parallel solid walls were fcc crystals and every pair of the nearest neighbors in the walls was bound through a harmonic potential $\Phi_h(r) = \frac{k}{2}(r - r_{\text{eq}})^2$, with r being the interparticle distance, $r_{\text{eq}} = 0.277$ nm, and $k = 46.8$ N/m. Interactions between fluid particles and between fluid and solid particles were modeled by a 12-6 LJ potential $\Phi^{\text{LJ}}(r_{ij}) = 4\epsilon_{ij} \left[\left(\frac{\sigma_{ij}}{r_{ij}} \right)^{12} - \left(\frac{\sigma_{ij}}{r_{ij}} \right)^6 \right]$, where r_{ij} was the distance between the particles i and j , while ϵ and σ denoted the LJ energy and length parameters, respectively. This LJ interaction was truncated at a cut-off distance of $r_c = 3.5\sigma$ and quadratic functions were added so that the potential and

interaction force smoothly vanished at r_c .²² We used the following parameters for fluid-fluid (ff) and solid-fluid (sf) interactions: $\sigma_{\text{ff}} = 0.340$ nm, $\epsilon_{\text{ff}} = 1.67 \times 10^{-21}$ J, $\sigma_{\text{sf}} = 0.345$ nm, $\epsilon_{\text{sf}} = 0.646 \times 10^{-21}$ J. The atomic masses of fluid and solid particles were $m_f = 39.95$ u and $m_s = 195.1$ u, respectively. Finally, the equations of motion were integrated using the velocity-Verlet algorithm, with a time step Δt of 5 fs.

The periodic boundary condition was set in the x and y -directions, and 4000 LJ particles were confined between two parallel solid walls consisting of the fcc crystal located on the bottom and top sides of the calculation cell, which directed (001) and (00-1) planes normal to the z -direction. Both had eight layers so that the possible minimum distance between the fluid particle and the solid particle in the outmost layer was longer than the cutoff distance. The relative positions of the solid particles in the outmost layers of each base crystal were fixed and the temperature of those in the second outermost layers was controlled at a control temperature of 100 K by using the standard Langevin thermostat.³³ The system was first equilibrated for 10 ns using the top wall as a piston with a control pressure of 4 MPa without shear so that a quasi-1D system with a LJ liquid confined between fcc solid walls was achieved. After the equilibration, further relaxation run to achieve a steady shear flow was carried out for 10 ns by moving the particles in the outmost layers of both walls with opposite velocities of ± 100 m/s in the x -direction, using the top wall as a piston with a control pressure of 4 MPa. Finally, steady shear flow simulation was carried out, keeping their z -position constant at the average position during the 2nd relaxation run, where the system pressure resulted in 3.61 MPa.

We tested the MoP expression (TABLE I) in the steady state, where the local density, velocity, advection term, and stress were obtained as the time-average of 200 ns on a grid with x -normal bin faces with a height $\Delta z = 0.150$ nm and z -normal ones with a width $\Delta x = 0.145$ nm. Assuming that the system is quasi-1D, the distribution in the x -direction was averaged for bins with identical z -positions. For a comparison, we also obtained the density and velocity distributions based on a standard volume average (VA), where the time-average in equally divided bin volumes parallel to the solid wall with a height of 0.15 nm were calculated.

Figure 1 (b) shows the distributions of density ρ and macroscopic velocity in the x -direction u_x calculated by the proposed MoP and standard VA as a reference. Note that these distributions by the MoP can be calculated both on x -normal bin faces and on z -normal

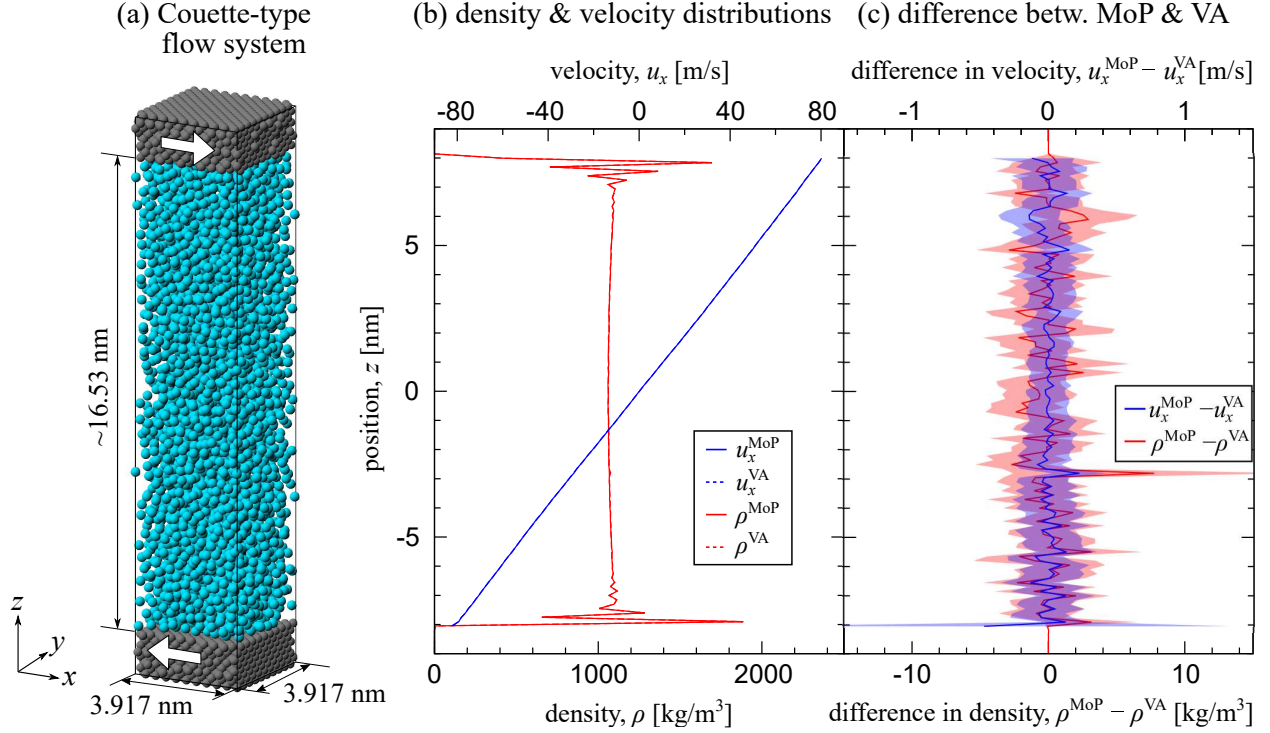


FIG. 1. (a) Quasi-1D Couette-type flow system of a Lennard-Jones liquid confined between two solid walls. (b) Distributions of density ρ and velocity u_x calculated by the proposed Method of Plane (MoP) and the volume average (VA). Solid and dashed lines denote the results of MoP and VA, respectively while the two lines almost overlap in this scale. (c) Difference between MoP and VA regarding density $\rho^{\text{MoP}} - \rho^{\text{VA}}$ and velocity $u_x^{\text{MoP}} - u_x^{\text{VA}}$ with their error bars depicted with semi-transparent areas around the average.

ones as shown later, while only the distributions obtained on x -normal bin faces are shown as the MoP results here. Overall, the MoP well reproduced the results by the VA, and the two lines almost overlap in this scale. Regarding the density distribution, except near the walls where layered structures are observed, bulk liquid with almost constant density was formed. Note that the bulk density was not completely constant because the temperature was not constant due to the viscous heat dissipation induced by the extreme shear imposed on this system. The shear velocity profiles are linear throughout almost all the liquid part except in layered structures, which can be understood by the change of local viscosity there. The density and velocity differences between MoP and VA are shown in Fig. 1 (c). The density difference was within 10 kg/m³, which is less than 1 % of the bulk density, and the

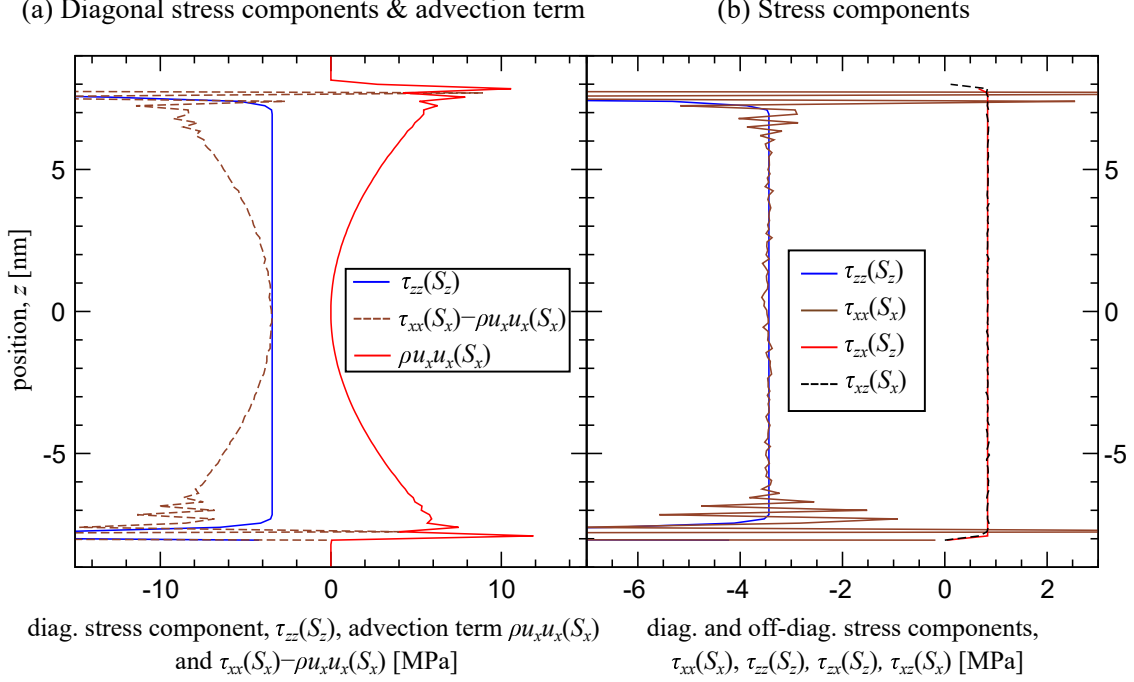


FIG. 2. Distributions of (a) the diagonal stress component $\tau_{zz}(S_z)(\equiv \tau_{zz}^{\text{int}} + \tau_{zz}^{\text{kin}})$, advection term $\rho u_x u_x(S_x)$ and $\tau_{xx}(S_x) - \rho u_x u_x(S_x)[\equiv \tau_{xx}^{\text{int}} + (\tau_{xx}^{\text{kin}} - \rho u_x u_x)]$, and (b) diagonal and off-diagonal stress components $\tau_{xx}(S_x)$, $\tau_{zz}(S_z)$, $\tau_{zx}(S_z)$ and $\tau_{xz}(S_x)$.

velocity difference was also within 0.5 m/s, showing that proposed MoP can extract the density and velocity distribution consistent with VA.

Figure 2 (a) shows the distributions of $\tau_{zz}(\equiv \tau_{zz}^{\text{int}} + \tau_{zz}^{\text{kin}})$, $\tau_{xx} - \rho u_x u_x[\equiv \tau_{xx}^{\text{int}} + (\tau_{xx}^{\text{kin}} - \rho u_x u_x)]$ and $\rho u_x u_x$, where the first two were directly obtained with simple addition based on Eqs. (9) and (21) as also listed in the top part of TABLE I, while $\rho u_x u_x$ was obtained from the density ρ and velocity u_x . Note that $\tau_{zz} - \rho u_z u_z$ is shown as τ_{zz} because u_z is equal to zero in the whole area of the present system. Also note that the calculation of τ_{kl}^{int} in Eq. (9) was the same as in equilibrium systems without macroscopic flow. As clearly observed, $\tau_{xx} - \rho u_x u_x$ including the advection and τ_{zz} are different away from the solid walls, indicating that the flow effect should be removed to properly evaluate the fluid stress. Figure 2 (b) displays the distributions of the stress component τ_{xx} , τ_{zz} , τ_{zx} and τ_{xz} , where τ_{zz} and τ_{zx} were calculated on z -normal bins whereas the others were obtained on x -normal bins. As explained above, the stress value τ_{xx} was calculated by adding $\rho u_x u_x$ to $\tau_{xx} - \rho u_x u_x$ whereas the advection terms for the others can be neglected considering $u_z = 0$. In the bulk region sufficiently

away from the walls, $\tau_{xx} = \tau_{zz}$ and $\tau_{zx} = \tau_{xz}$ are satisfied as expected from the solution of a laminar Couette flow, and the former indicates that the stress τ_{xx} is adequately calculated by the proposed MoP with the resulting value $-\tau_{xx}(= -\tau_{zz})$ equal to the external pressure value of 3.61 MPa. The wall-tangential diagonal stress τ_{xx} fluctuates near the walls as typically observed also in equilibrium systems,^{10,22} because of the layered structure of the liquid as displayed in the density distribution in Fig. 1 (b). On the other hand, τ_{zz} was constant except near the walls, where the solid-liquid (SL) interaction acts as the external force on the liquid. Regarding the off-diagonal components $\tau_{zx}(= \tau_{xz})$, they were constant except just around the walls, where friction from the solid is included in the force balance even in the laminar flow.

In addition to the normal velocity component u_k on the MoP plane S_k , the calculation of u_l ($l \neq k$) tangentially to S_k is needed for the separation of $\tau_{kl}^{\text{kin}}(S_k) - \rho u_l u_k(S_k)$ in Eq. (24) to properly define the stress in general flows with $u_l \neq 0$ and $u_k \neq 0$. Including this tangential velocity, we compared the distributions of the density ρ , the mass flux ρu_x and the velocity u_x averaged on x -normal and z -normal bin faces as another numerical test in the present system in Fig. 1. More concretely, the density $\rho(S_x)$ and $\rho(S_z)$ averaged on x -normal and z -normal bin faces S_x and S_z , respectively were calculated by Eq. (15) with setting $k = x$ and $k = z$, whereas the macroscopic mass flux $\rho u_x(S_x)$ and $\rho u_x(S_z)$ were obtained by Eq. (17) with $l = x$ on S_x and S_z , respectively. With these definitions, $u_x(S_x) \equiv \frac{\rho u_x(S_x)}{\rho(S_x)}$ on S_x as well as $u_x(S_z) \equiv \frac{\rho u_x(S_z)}{\rho(S_z)}$ on S_z can be obtained as in Eq. (18). Note that in the present laminar flow system with $u_z = 0$, the calculation of u_x is practically not needed for the stress separation for τ_{zz}^{kin} , τ_{zx}^{kin} and τ_{xz}^{kin} in Eq. (24). Figure 3 shows the distributions of the (a) density ρ , (b) mass flux ρu_x , and (c) velocity u_x defined on x -normal and z -normal bin faces, in the system in Fig. 1, where the values averaged on each bin face of x -normal and z -normal are plotted with setting the z -position at the center of each bin face, respectively, *i.e.*, they are staggered by $\Delta z/2$. In the bulk, ρ , ρu_x and resulting u_x averaged on bin faces with different normal directions agreed well, indicating that the separation of the stress and advection terms in Eq. (24) is possible with the velocity values properly evaluated by the proposed method. The difference seen around the top and bottom is due to the layered structures around the two walls, *i.e.*, the values on S_z are the average on a surface parallel to the layered structure whereas those on S_x are the average across the layers.

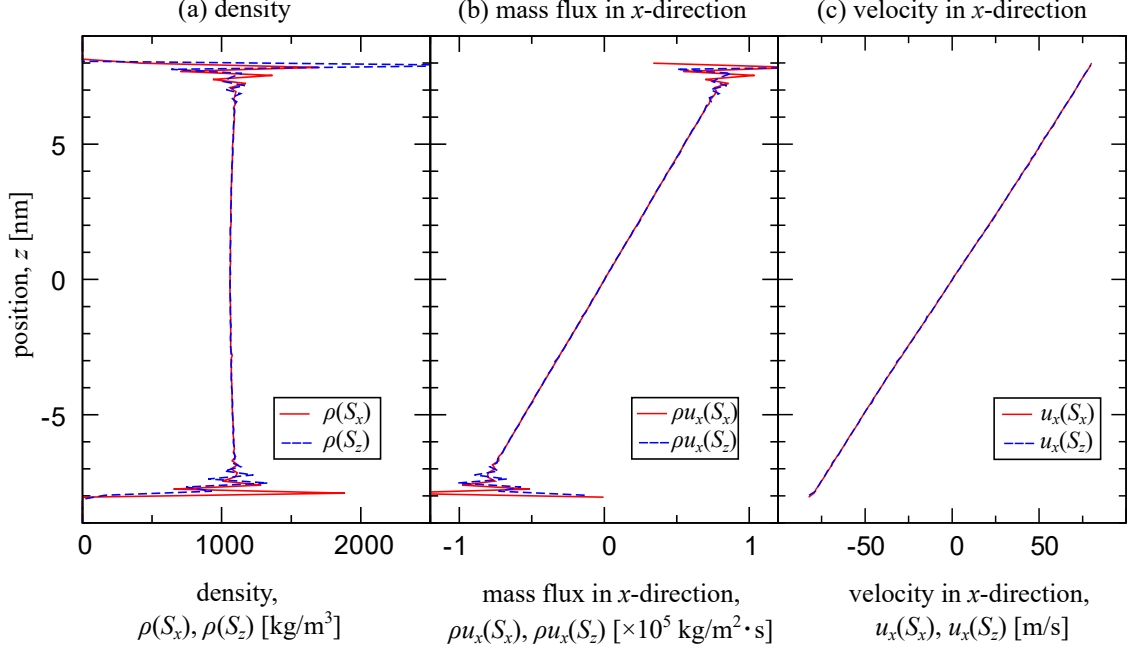


FIG. 3. Comparison of the time-averaged distributions of the (a) density ρ (b) mass flux ρu_x and (c) velocity u_x averaged on x -normal and z -normal bin faces S_x and S_z , respectively.

B. Quasi-2D shear flow with solid-liquid-vapor contact lines

The top panel of Fig. 4 shows the MD simulation system of a quasi-2D Couette-type flow, where the basic setups are the same as in the quasi-1D system. The periodic boundary condition was set in the x - and y -directions, and 20,000 LJ particles were confined between two parallel solid walls with a distance about 10.4 nm and a dimension of $x \times y = 3.92 \times 39.2 \text{ nm}^2$ so that the LJ fluid may form two quasi-2D menisci with contact lines on the walls upon the preliminary equilibration at a control temperature $T = 85 \text{ K}$ without shear. The static contact angle on both top and bottom walls were about 57 degrees. After the equilibration, further relaxation run to achieve a steady shear flow with asymmetric menisci were carried out for 10 ns by moving the particles in the outmost layers of both walls with opposite velocities of $\pm 10 \text{ m/s}$ in the x -direction.

After the relaxation run, the density, velocity and stress distributions were obtained by the present MoP expression in the steady state with the time-average of 500 ns on x -normal bin faces with a length of $\Delta z = 0.149 \text{ nm}$ and z -normal ones with a length of $\Delta x = 0.150 \text{ nm}$.

The middle panel of Fig. 4 shows the distributions of density ρ calculated on the x -normal

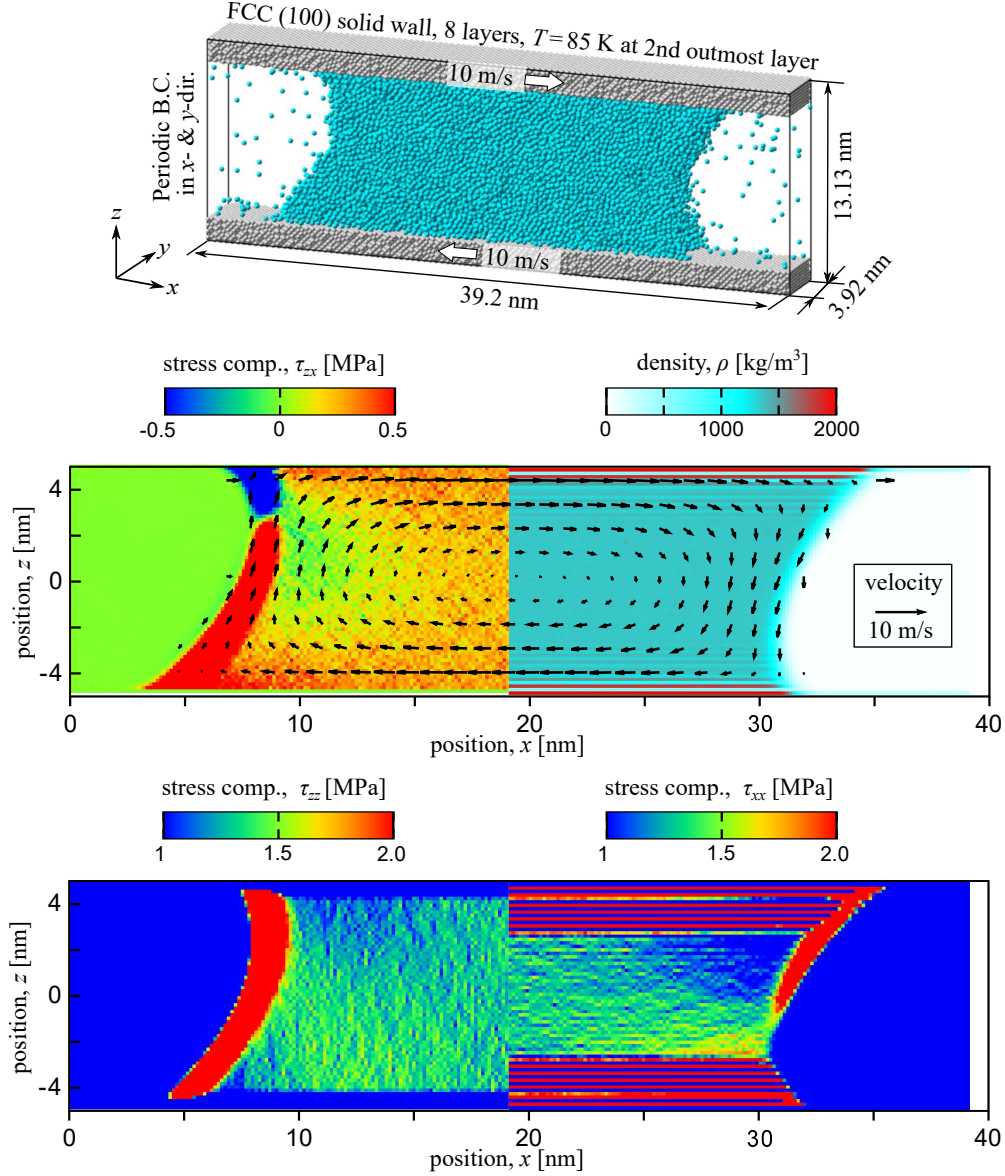


FIG. 4. Top: Quasi-2D Couette-type flow system of a Lennard-Jones liquid confined between two solid walls. Middle: Distributions of density ρ , velocity \mathbf{u} , and off-diagonal stress component τ_{zx} . Black arrow denotes the macroscopic velocity calculated by the proposed Method of Plane. Bottom: Distributions of diagonal stress components τ_{xx} and τ_{zz} .

bin faces, velocity vector with components calculated on each bin face corresponding the component direction, and a stress component τ_{zx} , where those for ρ and τ_{zx} are displayed only for the half of the system with respect to the center of mass of the fluid considering the symmetry. A clockwise caterpillar like flow is clearly captured by the present method,

where the shear stress τ_{zx} distribution in the liquid phase shows the non-uniformity of the viscous stress. The strong tensile stress seen in the τ_{zx} distribution around the LV interfaces is due to the LV interfacial tension. The bottom panel of Fig. 4 shows the distributions of diagonal stress components τ_{xx} and τ_{zz} . Layered structures are observed for τ_{xx} near the SL interfaces due to the adsorption layers in the density distribution. The relation between the density layers and stress distribution near the solid walls are qualitatively the same as in our previous study of static droplet:¹⁰ negative stress was seen in the adsorption layers, *i.e.*, the adsorption layers were compressed whereas tensile stress appeared between the layers.

Indeed, these apparent flow features can be qualitatively visualized by another methods such as atomic stress²⁴, but the present method provides the distributions of physical properties defined on a surface establishing a direct link with the conservation laws for arbitrary local volume as described in *Introduction*, and is generally applicable to a wide range of nanoscale systems with liquid flow. One of our future research targets is dynamic wetting³⁴⁻³⁶, for which we plan to examine the mechanical balance exerted on the fluid around a CV set around the moving contact line in Fig. 4. Through the comparison with the static case,¹⁰ this would enable the analysis of advancing and receding contact angle from a mechanical point of view.

IV. CONCLUDING REMARKS

In this work, we showed a calculation method of local stress tensor applicable to non-equilibrium MD systems based on the Method of Plane (MoP). From the relation between the macroscopic velocity distribution function and the microscopic molecular passage across a fixed control plane, we derived a basic equation to connect the macroscopic field variable and the microscopic molecular variable. Based on the connection, we derived a method to calculate the basic properties of the macroscopic momentum conservation law including the density, velocity and momentum flux as well as the interaction and kinetic terms of the stress tensor defined on a surface with a finite area. Any component of the streaming velocity can be obtained on a control surface, which enables the separation of the kinetic momentum flux into the advection and stress terms in the framework of the MoP. We verified the present method through the extraction of the density and velocity distributions by volume average (VA) and the MoP in a quasi-1D steady-state Couette flow system, seeing that the stress

tensor distribution by the MoP satisfies the solution of a laminar Couette flow in the bulk, indicating that the flow effect, *i.e.*, the advection term, was removed to evaluate stress properly. Furthermore, we showed the density, velocity, and stress tensor distributions by the MoP even in a quasi-2D steady-state system with a moving contact line. In our method as opposed to VA, the density, mass and momentum fluxes are defined on a surface, which is essential to have consistency with the conservation laws in dynamic systems.

ACKNOWLEDGMENTS

H.K., T.O. and Y.Y. are supported by JSPS KAKENHI Grant Nos. JP20J20251, JP18K03929, and JP18K03978, Japan, respectively. Y.Y. is also supported by JST CREST Grant No. JPMJCR18I1, Japan.

DATA AVAILABILITY

The data that support the findings of this study are available from the corresponding author upon reasonable request.

REFERENCES

- ¹J. H. Irving and J. G. Kirkwood, “The statistical mechanical theory of transport processes. IV. The equations of hydrodynamics,” *J. Chem. Phys.* **18**, 817–829 (1950).
- ²B. J. Alder and T. E. Wainwright, “Phase Transition for a Hard Sphere System,” *J. Chem. Phys.* **27**, 1208–1209 (1957).
- ³B. J. Alder and T. E. a. Wainwright, “Studies in Molecular Dynamics. I. General Method,” *J. Chem. Phys.* **31**, 459–466 (1959).
- ⁴D. Evans and G. Morriss, Statistical Mechanics of Nonequilibrium Liquids, 2nd ed. (Cambridge University Press, 2008) pp. 71–72.
- ⁵A. M. P. and T. D. J., Computer Simulation of Liquids, 2nd ed. (Oxford, 2017).
- ⁶D. H. Tsai, “The virial theorem and stress calculation in molecular dynamics,” *J. Chem. Phys.* **70**, 1375–1382 (1979).
- ⁷S. M. Thompson, K. E. Gubbins, J. P. R. B. Walton, R. A. R. Chantry, and J. S. Rowlinson, “A molecular dynamics study of liquid drops,” *J. Chem. Phys.* **81**, 530–542 (1984).

- ⁸B. D. Todd, D. J. Evans, and P. J. Daivis, “Pressure tensor for inhomogeneous fluids,” *Phys. Rev. E* **52**, 1627–1638 (1995).
- ⁹R. J. Hardy, “Formulas for determining local properties in molecular-dynamics simulations: Shock waves,” *J. Chem. Phys.* **76**, 622–628 (1982).
- ¹⁰Y. Yamaguchi, H. Kusudo, D. Surblys, T. Omori, and G. Kikugawa, “Interpretation of Young’s equation for a liquid droplet on a flat and smooth solid surface: Mechanical and thermodynamic routes with a simple Lennard-Jones liquid,” *J. Chem. Phys.* **150**, 044701 (2019).
- ¹¹J. F. a. Lutsko, “Stress and elastic constants in anisotropic solids: Molecular dynamics techniques,” *Journal of Applied Physics* **64**, 1152–1154 (1988).
- ¹²J.-G. Weng, S. Park, J. R. Lukes, and C.-L. Tien, “Molecular dynamics investigation of thickness effect on liquid films,” *J. Chem. Phys.* **113**, 5917–5923 (2000).
- ¹³J. Cormier, J. M. Rickman, and T. J. Delph, “Stress calculation in atomistic simulations of perfect and imperfect solids,” *Journal of Applied Physics* **89**, 99–104 (2001).
- ¹⁴D. M. Heyes, E. R. Smith, D. Dini, and T. A. Zaki, “The equivalence between volume averaging and method of planes definitions of the pressure tensor at a plane,” *J. Chem. Phys.* **135** (2011), 10.1063/1.3605692.
- ¹⁵J. Z. Yang, X. Wu, and X. Li, “A generalized Irving-Kirkwood formula for the calculation of stress in molecular dynamics models,” *J. Chem. Phys.* **137** (2012), 10.1063/1.4755946, 84870207982.
- ¹⁶D. M. Heyes, D. Dini, and E. R. Smith, “Equilibrium fluctuations of liquid state static properties in a subvolume by molecular dynamics,” *J. Chem. Phys.* **145**, 104504 (2016).
- ¹⁷E. R. Smith, D. M. Heyes, and D. Dini, “Towards the Irving-Kirkwood limit of the mechanical stress tensor,” *J. Chem. Phys.* **146**, 224109 (2017).
- ¹⁸K. Shi, E. E. Santiso, and K. E. Gubbins, “Can we define a unique microscopic pressure in inhomogeneous fluids?” *J. Chem. Phys.* **154**, 84502 (2021).
- ¹⁹E. R. Smith and C. Braga, “Hydrodynamics across a fluctuating interface,” *J. Chem. Phys.* **153**, 134705 (2020).
- ²⁰G. Bakker, Kapillarität und Oberflächenspannung, Vol. 6 (Wien-Harms, 1928).
- ²¹J. S. Rowlinson and B. Widom, Molecular Theory of Capillarity (Dover, 1982).
- ²²S. Nishida, D. Surblys, Y. Yamaguchi, K. Kuroda, M. Kagawa, T. Nakajima, and H. Fujimura, “Molecular dynamics analysis of multiphase interfaces based on in

- situ extraction of the pressure distribution of a liquid droplet on a solid surface,” *J. Chem. Phys.* **140**, 074707 (2014).
- ²³D. Surblys, Y. Yamaguchi, K. Kuroda, M. Kagawa, T. Nakajima, and H. Fujimura, “Molecular dynamics analysis on wetting and interfacial properties of water-alcohol mixture droplets on a solid surface,” *J. Chem. Phys.* **140**, 034505 (2014).
- ²⁴A. P. Thompson, S. J. Plimpton, and W. Mattson, “General formulation of pressure and stress tensor for arbitrary many-body interaction potentials under periodic boundary conditions,” *J. Chem. Phys.* **131**, 1–6 (2009).
- ²⁵S. Plimpton, “Fast Parallel Algorithms for Short-Range Molecular Dynamics,” *J. Comp. Phys.* **117**, 1–19 (1995).
- ²⁶H. Kusudo, T. Omori, and Y. Yamaguchi, “Extraction of the equilibrium pinning force on a contact line exerted from a wettability boundary of a solid surface through the connection between mechanical and thermodynamic routes,” *J. Chem. Phys.* **151**, 154501 (2019).
- ²⁷Y. Imaizumi, T. Omori, H. Kusudo, C. Bistafa, and Y. Yamaguchi, “Wilhelmy equation revisited: A lightweight method to measure liquid–vapor, solid–liquid, and solid–vapor interfacial tensions from a single molecular dynamics simulation,” *J. Chem. Phys.* **153**, 034701 (2020).
- ²⁸H. C. Andersen, “Rattle: A ”velocity” version of the shake algorithm for molecular dynamics calculations,” *J. Comput. Phys.* **52**, 24–34 (1983).
- ²⁹D. Surblys, H. Matsubara, G. Kikugawa, and T. Ohara, “Application of atomic stress to compute heat flux via molecular dynamics for systems with many-body interactions,” *Phys. Rev. E* **99**, 1–6 (2019).
- ³⁰P. J. Davis, K. P. Travis, and B. D. Todd, “A technique for the calculation of mass, energy, and momentum densities at planes in molecular dynamics simulations,” *J. Chem. Phys.* **104**, 9651–9653 (1996).
- ³¹K. Ogawa, H. Oga, H. Kusudo, Y. Yamaguchi, T. Omori, S. Merabia, and L. Joly, “Large effect of lateral box size in molecular dynamics simulations of liquid-solid friction,” *Phys. Rev. E* **100**, 023101 (2019).
- ³²H. Oga, Y. Yamaguchi, T. Omori, S. Merabia, and L. Joly, “Green-Kubo measurement of liquid-solid friction in finite-size systems,” *J. Chem. Phys.* **151**, 054502 (2019).
- ³³J. Blömer and A. E. Beylich, “Molecular dynamics simulation of energy accommodation of internal and translational degrees of freedom at gas–surface interfaces,” *Surf. Sci.* **423**,

127–133 (1999).

³⁴Y. Hizumi, T. Omori, Y. Yamaguchi, and T. Kajishima, “Study on the Navier boundary condition for flows with a moving contact line by means of molecular dynamics simulation,” *Trans. JSME (in Japanese)* **81**, 15–00409 (2015).

³⁵T. Omori, Y. Kobayashi, Y. Yamaguchi, and T. Kajishima, “Understanding the asymmetry between advancing and receding microscopic contact angles,” *Soft Matter* **15**, 3923–3928 (2019).

³⁶J. J. Thalakkttor and K. Mohseni, “Role of the rate of surface dilatation in determining microscopic dynamic contact angle,” *Phys. Fluids* **32**, 012111 (2020).